Dmitri N. Gavrilov
Boris Gorbovitski
Mikhail Gouzman
Georgiy Gudkov
Andrei Stepoukhovitch
Victor Ruskovoloshin
Andrei Tsuprik
Georgiy Tyshko
Olga Bilenko
Olga Kosobokova
Serge Luryi
Vera Gorfinkel

Department of Electrical
and Computer Engineering,
State University of New York,
Stony Brook, NY, USA

Dynamic range of fluorescence detection and base-calling accuracy in DNA sequencer based on single-photon counting

Recently, we developed a family of high-performance automated capillary DNA sequencing instruments based on a single-photon detection of fluorescently labeled DNA fragments. Our machines employ digital and broadband techniques, essential for achieving superior instrument sensitivity and dynamic range. In the present paper, we discuss limitations of the instrument's performance caused by the nonlinearity of single-photon detectors as well as methods for nonlinearity compensation which increase the detection dynamic range and base-calling accuracy.

1 Introduction

Capillary electrophoresis is widely used for the high-throughput DNA sequencing. Modern commercial sequencing machines employ a multicapillary format (ABI PRIZM-3100, CEQ-2000, ABI PRIZM-3700, MegaBACE). The highest number of lanes (384) is offered by the MegaBACE-4000 sequencer. At the same time, several groups have developed new high-throughput sequencing machines based on integrated-system technologies and prepare to overcome the 1000 channel barrier [1–10]. Miniaturization of multichannel devices using microfabricated capillary arrays is another important direction in the development of DNA sequencers [11–16]. Practically in all DNA sequencers, fluorescence labeling techniques are used for sequence detection. By their technical principle, the fluorescence detection systems used in current DNA sequencing instruments are very similar to those developed in the mid 1980s–1990s. They excite fluorescence markers using a laser source and then capture fluorescence with an analog photodetector (either of photomultiplier tube (PMT) or CCD type). The obtained signal is then digitized, transferred to a computer, and analyzed to determine the sequence. There are two major technical shortcomings common to all four-color machines: relatively low detection sensitivity and relatively narrow dynamic range, limited by used analog-to-digital conversion circuitry.

Correspondence: Dr. Dmitri N. Gavrilov, Department of Electrical and Computer Engineering, SUNY, Stony Brook, NY 11794-2350, USA
E-mail: gavrilov@ece.sunysb.edu
Fax: +631-632-5745

Abbreviations: PMT, photomultiplier tube; **SPD**, single-photon detector/detection

A number of extremely sensitive fluorescence detection techniques are available based on registering single-photons [17–20] commonly referred to as the single-photon detection (SPD) techniques. Because of their complexity and cost, SPD techniques were mostly used for specialized scientific applications, such as time-resolved fluorescence spectroscopy or detection of single fluorescent molecules [21–24]. Recently, our research group has demonstrated the first automated DNA sequencing instruments based on SPD technique ([25, 26]; Bilenko *et al.*, submitted). The instruments possess an ultra high sensitivity and a large detection dynamic range. In the present article, we will describe the nonlinear behavior of SPD systems causing limitations in the instrument performance. We will also discuss nonlinearity mechanisms and different approaches to nonlinearity compensation which enable a significant increase of the instrument dynamic range and which improve base-calling accuracy.

2 Materials and methods

2.1 Models of nonlinearity in SPDs

2.1.1 SPDs

The SPD, also referred to as single-photon counting head, is a device that produces single electric pulses as a response to incident photons (one pulse per one photon). Single-photon sensitive detectors typically used for SPDs are either PMTs or avalanche photodiodes (APD). In the present paper we will focus on PMT-based SPDs. The block diagram of a typical SPD is shown in Fig. 1. An incident photon flux impinged onto a photocathode of a PMT produces a stream of short nano-
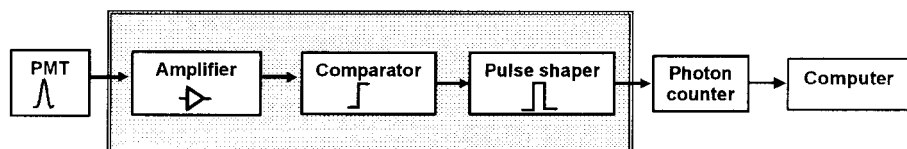
Figure 1. Block diagram of an SPD.

second current pulses on the PMT output. These pulses are amplified by a fast pulse amplifier. If the amplitude of an individual pulse exceeds a certain threshold, the pulse is selected by a comparator and further shaped by a pulse shaper which produces output voltage pulses of predetermined width and height. Shaped pulses are counted by a digital counting circuit. The obtained information is transferred to a computer where it is recorded and processed. In the present article, we will discuss two SPD systems: commercial single-photon PMT detectors with built-in pulse processing electronic circuit (Hamamatsu H6240-02 and H7467; pulse resolution 35 and 70 ns, correspondingly), and an SPD system using PMT Hamamatsu H7260 with our home-designed electronic circuit which provides the pulse resolution of about 9 ns.

2.1.2 Models of SPD nonlinearity

In an ideal SPD with zero pulse width, the output pulse rate is strictly proportional to the incident light intensity $I(t)$ for any intensity in the interval $0 < I < \infty$:

$$R_{ideal}(t) \sim I(t) \qquad (1)$$

The number of pulses registered per time interval has Poisson distribution. Time intervals between consecutive pulses are distributed exponentially with a mean value $\bar{\tau} = 1/R_{ideal}$. In contrast to ideal devices, real SPDs always have limited temporal resolution mostly because of the finite width of the electric pulses produced in response to incident photons. Therefore, there is a minimum time interval between two consecutive incident photons that can be individually registered by the SPD. Increase in the photon arrival rate causes growth of the percentage of lost counts and, therefore, nonlinearity of the SPD response. An accurate mathematical description of SPD characteristics in a wide range of nonlinearity is extremely difficult due to the complexity of the physical processes in PMT and amplification circuits. Below, we consider three simplified models which describe nonlinear behavior of different SPD types.

2.1.2.1 Fixed 'dead' time model (Model I)

This model represents the classic approach to SPD analysis. The model assumes that after each registered photon there is a fixed 'dead' time τ_d. All photons, arriving

during τ_d after the registered photon, are ignored by the detection system. This system's behavior is caused by a specific design of the SPD electronic circuit: once triggered by the first arrived photon, the circuit discards electric pulses produced by all following photons which arrive during the fixed dead-time interval τ_d. Statistical properties of the output data are discussed in detail in [27]. The relationship between registered count rate R_{reg} and true count rate R_{ideal} is expressed as:

$$R_{reg} = \frac{R_{ideal}}{1 + \tau_d R_{ideal}} \qquad (2)$$

Analysis of Eq. (2) shows, that $R_{reg} \rightarrow 1/\tau_d$ at $R_{ideal} \rightarrow \infty$, which means saturation of the registered count at high photon arrival rates. The above equation can be easily inverted into a form convenient for linearization of SPD output data:

$$R_{ideal} = \frac{R_{reg}}{1 - \tau_d R_{reg}} \qquad (3)$$

The simplicity of the equation which relates true count R_{ideal} and registered count R_{reg} makes this model attractive for application in computational linearization algorithms.

2.1.2.2 Fixed temporal resolution model (Model II)

This model was proposed in [28] for the description of the ultrafast SPD systems designed and implemented by our research group in the course of the development of DNA sequencer based on SPD (Bilenko *et al.*, submitted). This model is applicable to photon counting circuits which do not comprise the pulse shaper. Such a circuit design can be used for decreasing the circuit response time and increasing the SPD dynamic range. In such systems two consecutive photons can only be counted if the time interval between their arrivals is larger than certain time τ_{res}. All the photons following the one that starts the interval τ_{res} and falling into the τ_{res} are lost (not registered by the detection system). However, in contrast to the fixed dead-time model, each lost photon becomes a starting point for a new interval τ_{res}. Thus, effective "dead" time of the SPD in this model depends on the count rate. Once the time interval after arrival of a photon exceeds τ_{res}, the system is ready for

the registration of the next arriving photon. The relationship between registered count rate R_{reg} and the true count rate R_{ideal} is expressed as:

$$R_{reg} = R_{ideal} \exp\{-\tau_{res} R_{ideal}\} \tag{4}$$

(see Addendum 1, p. 1192 for derivation of the Eq. 4). The maximum photocount rate which can be registered by the system is

$$R_{max\,reg} = 1/(e\tau_{res}) \tag{5}$$

This rate is observed at the ideal count rate

$$R_{max\,ideal} = 1/\tau_{res} \tag{6}$$

Further increase in photon arrival rate R leads to the reduction in the registered photocount rate. We define nonlinearity $L^\%$ of the SPD system as:

$$L^\% = \frac{R_{ideal} - R_{reg}}{R_{ideal}} 100\% \tag{7}$$

Thus, nonlinearity $L^\%$ is zero for $R_{ideal} = R_{reg}$. According to the fixed temporal resolution model, SPD system registers its maximum count at nonlinearity $L^\% = 61.4\%$ for any τ_{res}.

2.1.2.3 Combined model (Model III)

This model combines the features of both previous models. The photon registration system can be described as having two states: "high" and "low". Transition from "low" to "high" state represents the count registration event. After a photon is registered, the system stays for τ_H in "high" state and then returns to the "low" state. Similarly to the fixed time resolution model, photons, arriving when the registration system is already in its "high" state extend the system stay in the "high" state. If no photons arrive during the time interval τ_H, the registration system returns to its "low" state. After the transition to the "low" state the system discards all photons which arrive during the period of τ_L. After this, the system registers the first arrived photon which simultaneously causes the system's transition from "low" to "high" state. Thus, while the system "lifetime" in the "high" state, τ_H depends on the intensity of the incident photon flux, the "low" state "lifetime" τ_L is intensity-independent. This type of system behavior is characteristic to SPD systems having no pulse shaper in the amplifying circuit and having certain delay time due to a comparator fall time. The relationship between registered count R_{reg} and true count R_{ideal} rate in the combined model is:

$$R_{reg} = \frac{R_{ideal}}{\tau_L R_{ideal} + \exp\{\tau_H R_{ideal}\}} \tag{8}$$

(see Addendum 2, p. 1192 for derivation of the Eq. 8). This function reaches its maximum

$$R_{max\,reg} = 1/(\tau_L + e\tau_H) \tag{9}$$

at true photocount rate

$$R_{max\,ideal} = 1/\tau_H$$

Corresponding nonlinearity

$$L^\% = \left(1 - \frac{k}{1 + ek}\right)100\%$$

where $k = \tau_H/\tau_L$.

In particular case when $\tau_L = \tau_H$

$$L^\% = \frac{e}{1 + e} 100\% = 73.1\% \tag{10}$$

Figure 2a presents a nonlinear SPD response which is calculated using Eqs. (3), (4), and (8) for the above three models. The characteristics of Models I and II were calculated using $\tau_d = \tau_{res} = 70$ ns and for Model III we used $\tau_H = \tau_L = 35$ ns. The plots show the close match between all three curves at low count rates. The difference in the registered count rate between Models II and I (Fig. 2b) does not exceed 1% for nonlinearity below 15%. For Models III and I the difference in registered count rate
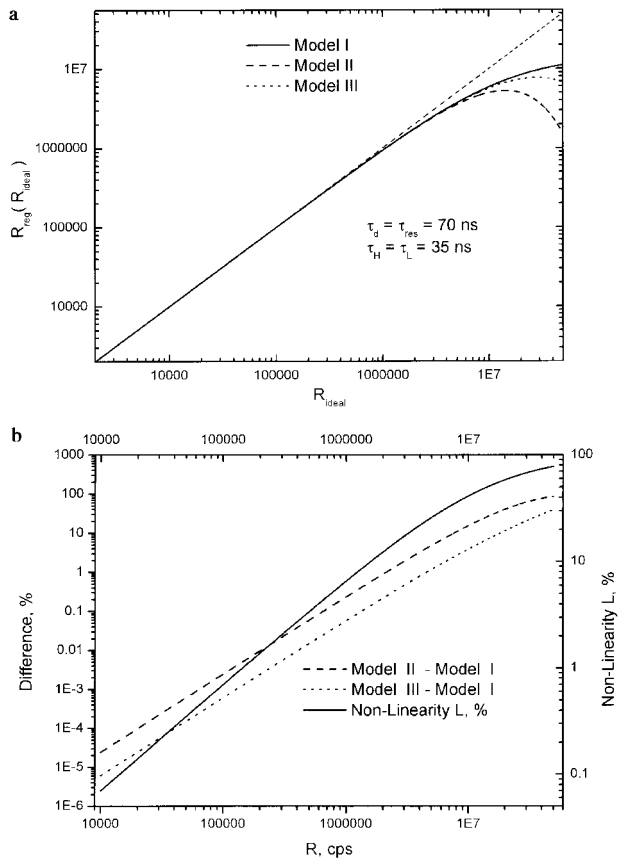
Figure 2. (a) Monte-Carlo simulation of the SPD response for three nonlinearity models. $\tau_d = \tau_{res} = 70$ ns for Models I and II, $\tau_H = \tau_L = 35$ ns for Model III. (b) Difference in registered count rate between Model I and Models II and III.

stays below 1% up to 25% nonlinearity. Thus, for nonlinearity within 15% range, the simple Model I can be used for approximation of SPD systems described by more complex models.

2.2 Methods for characterization of single-photon counters

Experimental characterization of an SPD includes measurement of its count rate depending on an incident photon flux, selection of a model, and evaluation of the model parameters. Model selection is performed by analyzing the SPD circuits. Model parameters can be obtained either from specially designed calibration experiments or extracted from measured SPD characteristics using the best fit between measured characteristics and a selected model. Below we consider two SPD characterization methods.

2.2.1 Statistical distribution analysis method

This method is based on the fact that limited temporal resolution of an SPD causes deviation of the shape of probability density function (PDF) of the SPD output data from the shape of Poisson distribution. The probability density function can be obtained for any fixed illumination intensity by recording the SPD output count and computing its histogram. The intensity of the incident light at the SPD input must be high enough for the SPD to operate in the nonlinear region of its characteristics, and the length of the data set must be sufficient to obtain a high quality histogram. The description and analysis of algorithms which implement the method are presented in [28]. A series of guesses about the 'dead' time value $\hat{\tau}_d$ is made and a theoretical histogram is calculated for each $\hat{\tau}_d$. The value of $\hat{\tau}_d$ that provides minimum mismatch between experimental and theoretical histograms is selected as an estimate of the system 'dead' time. Testing of the method showed that it provides appropriate quality estimates when the SPD operates with nonlinearity over 3%. Unfortunately, the equation for theoretical PDF that describes the statistical properties of the output data of an SPD is available only for the system described by Model I. For Models II and III the method can only be applied for nonlinearity varying within a narrow percent range.

2.2.2 Best fit method

In this method, the model parameters are extracted from measured SPD characteristics using the best fit between obtained characteristics and the selected model. It is important to note that the direct measurement of SPD

characteristics in the range from 1000 to 100 million counts per second (cps) is a rather complicated task since it requires an accurate measurement of incident light intensity in 50 dB dynamic range with ∼1% accuracy. In order to circumvent this difficulty, we designed a special experimental setup recording pairs of data points keeping constant a ratio of used light intensity values (if n_{th} pair is recorded using intensities I_n and wI_n, then $(n + 1)_{th}$ pair is recorded using light intensities I_{n+1} and wI_{n+1}, where w is a constant). The experimental setup used to obtain such data comprised a stabilized laser light source, a set of neutral optical filters, a fixed ratio attenuator and a slot for calibrated photodetector. The set of filters was used to select intensity I_n in wide range. The attenuator that allows a switch between two transmission coefficients 1 and w, is positioned in front of the photodetector and is used to form data pairs (I_n, wI_n). Total N pairs of data points are recorded at various light intensities over the whole dynamic range of the SPD. Let us assume that rate values $R_{reg\ n1}$ and $R_{reg\ n2}$ belonging to the n_{th} pair and are recorded with light intensities I_n and wI_n, where $n \in [1, N]$. We denote the direct and inverted characteristics of SPD given by the selected model as $f(\cdot)$ and $f^{-1}(\cdot)$:

$$R_{reg} = f(\hat{R}_{ideal}) \tag{11}$$

$$\hat{R}_{ideal} = f^{-1}(R_{reg}) \tag{12}$$

Then, the ratio w_n of estimates of ideal count rate $\hat{R}_{ideal\ n1}$ and $\hat{R}_{ideal\ n2}$ for n_{th} pair of values can be expressed as:

$$w_n = \frac{\hat{R}_{ideal\ n2}}{\hat{R}_{ideal\ n1}} = \frac{f^{-1}(R_{reg\ n2})}{f^{-1}(R_{reg\ n1})} \tag{13}$$

Parameters of the model are chosen by minimization of the sum of absolute values of deviations of w_n from its median value w_{MED}:

$$\sum_{n=1}^{N} |w_n - w_{MED}| \rightarrow \min \tag{14}$$

While closed form representation for $f^{-1}(\cdot)$ can be easily found for Model I, estimates of $\hat{R}_{ideal}$ for Models II and III can be obtained only numerically.

2.3 Nonlinearity compensation

Compensation of the nonlinearity of SPD systems can be performed numerically by computing an estimated ideal photocount rate $\hat{R}_{ideal}$ using measured values of rate R_{reg}. For Model I, alinearization procedure can be performed for registered count rates in the range of $R_{reg}\tau_D < 1$. For SPD systems described by Models II and III linearization is only possible in the range of count rates in which the characteristics are growing monotonously, *i.e.*, in the range limited by $R_{ideal} \in [0, R_{max\ ideal}]$ and $R_{reg} \in [0, R_{max\ reg}]$.

The computational procedure used for linearization is based on implementation of Eq. (12). Note that each model will be characterized by a specific characteristic *f*. While linearization for Model I can be easily implemented (Eq. 3), Models II and III require more complicated numerical computational algorithms for inversion of Eqs. (4) and (8).

3 Results and discussion

3.1 Characterization of SPDs

3.1.1 Measurement of characteristics of SPDs

The experimental setup used for measurement comprised a stabilized light source coupled to SPD through a calibrated tunable attenuator *via* optical fibers. The attenuator with a built-in set of neutral optical filters provided attenuation in the range from 0 to 90 dB. Registered values of photocount rate *versus* attenuation coefficient are shown in Fig. 3. In order to extract model parameters and apply linearization algorithms, monotonously increasing regions of measured SPD characteristics were approximated using the described models.
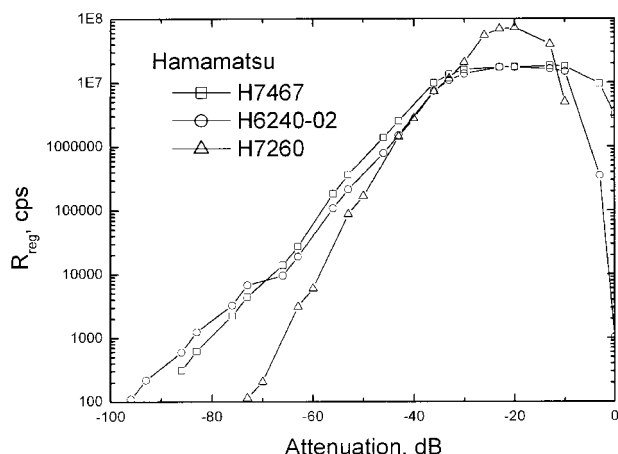
Figure 3. Measured characteristics of three single-photon counting heads Hamamatsu H7467, H6240-02, and H7260 PMT *versus* attenuation of the controlled light source.

3.1.2 Model selection

Hamamatsu H6240-02 and H7467 single photon counting heads: The behavior of these SPDs is primarily determined by the properties of built-in pulse shapers. Both SPDs exhibit saturation of the registered count rate at high illumination intensities. Therefore, we have concluded that both devices fall into the category described

by the Model I. Hamamatsu 7260 single photon counting head: The electronic circuit of the SPD based on PMT H7260 was designed by us to obtain the fastest device response using commercial microcircuits. The circuit does not contain a pulse shaper and its response time is primarily determined by the raise/fall time characteristic of the fast comparator used in the SPD amplifier. Oscillograms of the output signal at the PMT and comparator terminals are shown in Fig. 4. The recording was performed at counting rates in the range of $5 \times 10^7 - 7 \times 10^7$
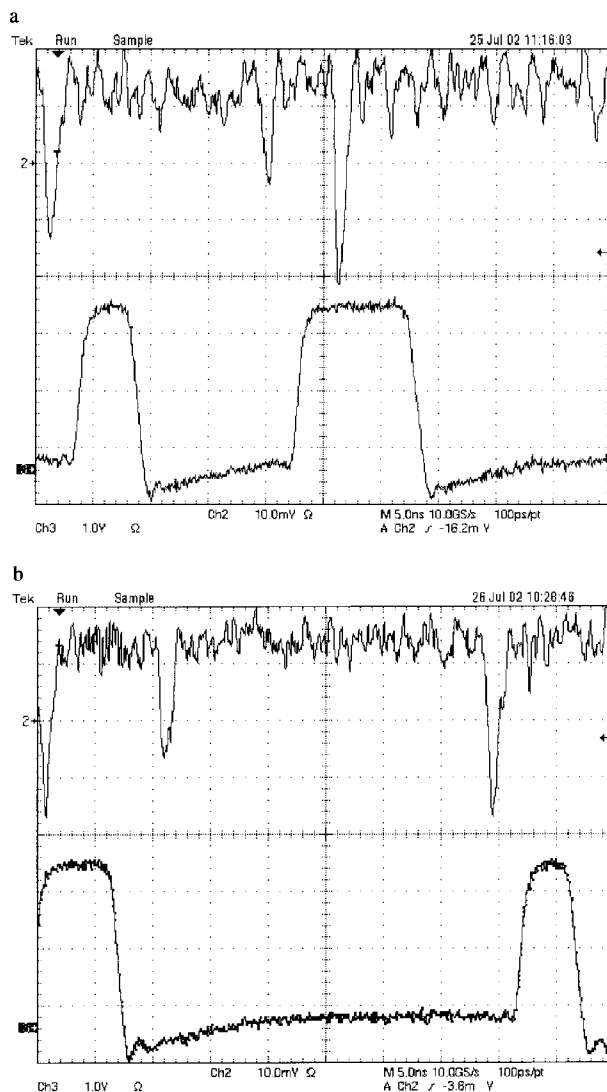
Figure 4. Oscillograms of output signals from PMT (Hamamatsu H7260) (negative pulses at the top of the screen) and after the comparator (positive pulses at the bottom of the screen). (a) Illustrates merging of pulses with time τ_H between them when the comparator is in its 'high' state, which is typical behavior for Model II system. (b) Illustrates loss of pulses falling into τ_L following the transition of the comparator to its 'low' state, which is typical to the behavior of Model I.

counts per second using Tektronix TDS 7404 Digital Oscilloscope. Output of the PMT is represented by negative polarity pulses at the top of the screen and the output of the comparator is shown as positive pulses at the bottom of the screen. The plots show merging pulses with time less than τ_H when the comparator is in its 'high' state (Fig. 4a) and missing pulses fall into τ_L in its 'low' state, demonstrating behavior typical for Model III.

3.1.3 Parameter estimation

An estimation of model parameters was performed using the 'best fit' method. The parameters of Model I were estimated using experimental data obtained from SPD's H7467 and H6240-02. The results of the fitting are shown in Figs. 5a and c. The best fit was achieved for the model with 'dead' time $\tau_d = 58$ ns for H7467 and $\tau_d = 42$ ns for H6240-02, correspondingly. Figures 5b and d show the

percent difference D between the approximating model and experimental data points. Mismatch D between data points and approximated characteristics of H6240-02 does not exceed 2.5% with overall mean square error $MSE = 1.53$ in the range of nonlinearity up to 60%. Model I describes characteristics of H7467 with $MSE = 2.69$. Comparison of Figs. 5b and d shows that for both SPDs Model I provides a good fit of characteristics. We fitted both Model I and Model III to data points obtained from H7260 SPD. The results are presented in Fig. 6. The best fit was achieved using Model I with $\tau_d = 9$ ns (Fig. 6a). Model III gave the best fit with parameters $\tau_H = 3.52$ ns and $\tau_L = 4.22$ ns (Fig. 6c). The comparison of Figs. 6b and d shows significant advantages of Model III over Model I. The mismatch given by using Model III does not exceed 5% with $MSE = 0.67$ in the whole range of nonlinearity up to 80%, whereas mismatch obtained with Model I reaches 13% at the top of the region with $MSE = 2.28$.
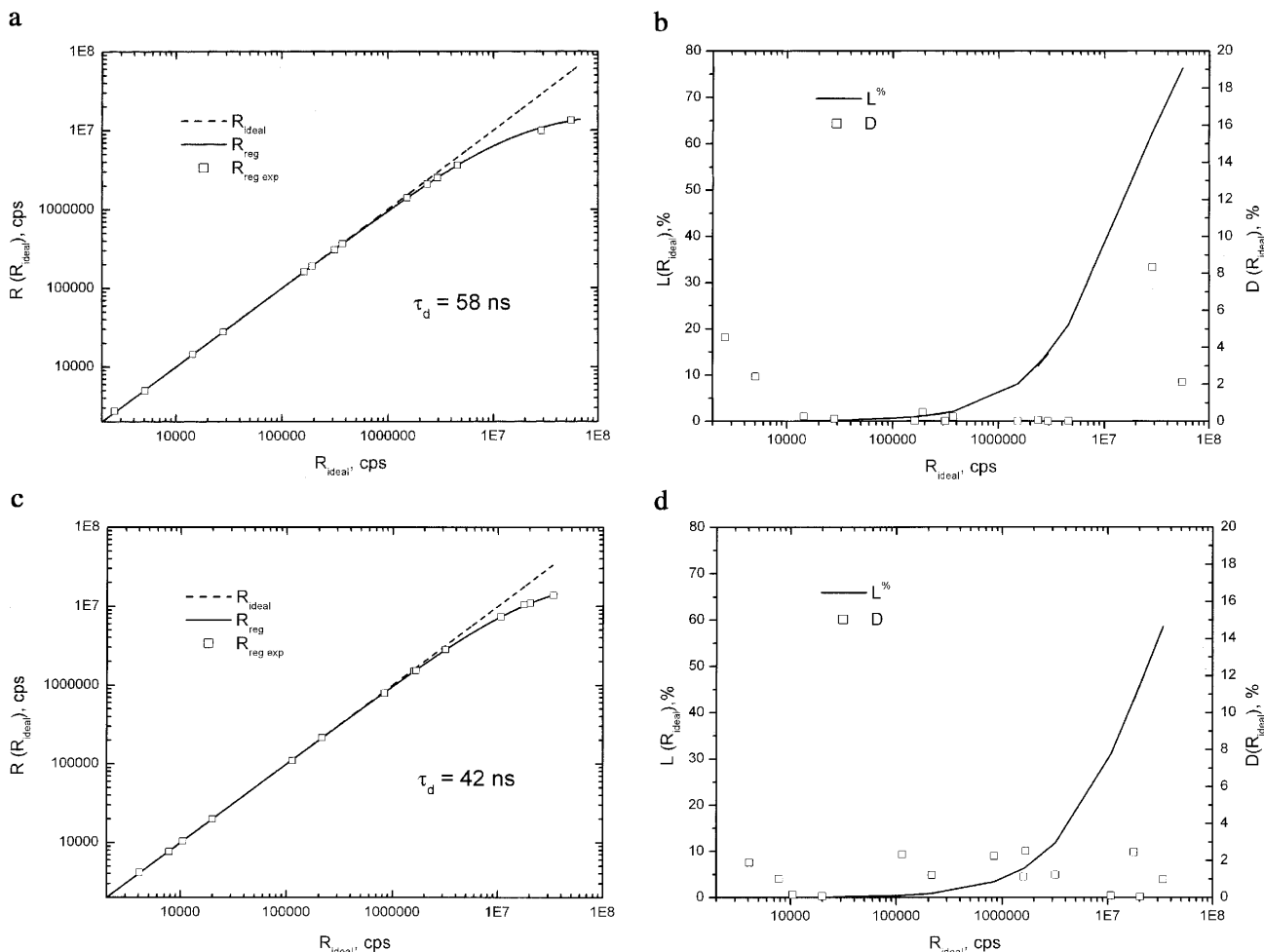
Figure 5. Fitting of measured data points for (a) H7260 and (c) H624002 detectors to Model I and deviation of data points from the approximating models (b) H7260 and (d) H6240-02.

a

b

c

d
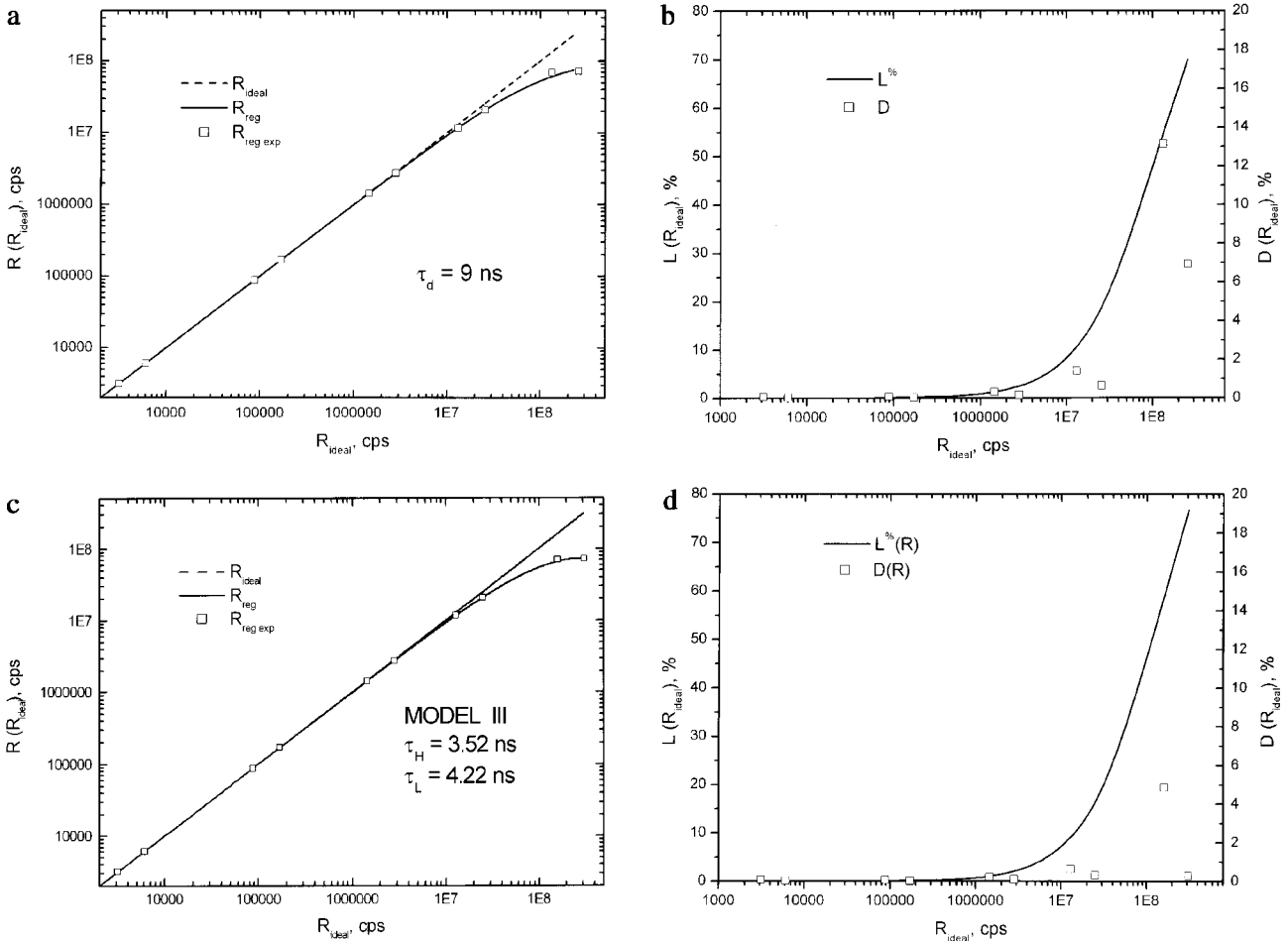
Figure 6. Fitting of (a) Model I and (c) Model III to measured data points from Hamamatsu H7260 detection head and deviation of data points from approximating models (b) Model I and (d) Model III.

3.2 Cross-talk linearization in DNA sequencing data processing

In DNA sequencing, four traces of data, corresponding to four spectral ranges of detected fluorescence signal, are used to perform a base-calling. Cross-talk between channels due to numerous factors causes correlation between the traces [30]. Linear transformation is commonly used to remove the channel cross-talk. Obviously, nonlinearity of the photodetector causes a distortion of the recorded data and introduces inaccuracy into the cross-talk removal procedure. In order to eliminate the data distortion introduced by the SPD nonlinearity and restore the base-calling accuracy, we used the linearization technique described in the previous sections.

Figure 7 shows the effect of linearization on cross-talk matrix at different photocount rates. The data set was recorded using SBS-2000 sequencer [26] and H7467
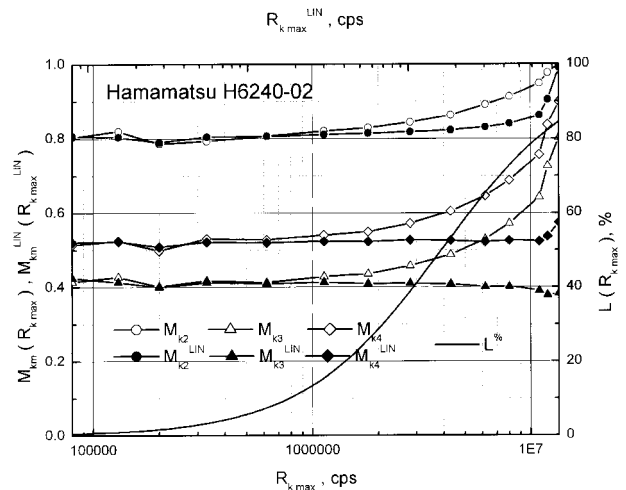
Figure 7. Drift of measured M_{km} and linearized M_{km}^{LIN} matrix coefficients with increase of registered $R_{k\,max}^{LIN}$ count rate and corresponding growth of nonlinearity $L^\%$ in the system.

detector. A sample containing a rhodamine dye diluted in distilled water was placed in the capillary. A Nd:YAG laser (532 mn) was used for fluorescence excitation. The illumination intensity was varied using optical filters at the laser output. The excited fluorescence signal passed through a rotating filter wheel comprising four band-pass filters (545 $\pm$ 5 nm, 560 $\pm$ 5 nm, 590 $\pm$ 5 nm, 610 $\pm$ 5 nm), and values of count rate R_{km} were obtained through each of the four filters (m = 1,2,3,4) at intensity level k and recorded by a computer in four different channels. Due to a certain shape of the dye emission spectrum, the ratio of fluorescence intensity in any particular spectral channel to maximum fluorescence intensity (always obtained through 560 nm filter) remained constant for low illumination intensities (in the linear detection range). For higher illumination intensities corresponding to SPD nonlinear behavior (nonlinearity exceeding 15%), the ratio of fluorescence intensity in different channels deviated from its linear value (see Fig. 7). In order to compensate the nonlinearity effect we used Model I with the parameter τ_d = 58 ns. A linearized value of the counting rate R_{km}^{LIN} for each measured value R_{km} was calculated using Eq. (3). Recorded and linearized data values were normalized for each intensity level to the count rate value $R_{k\,max}$ obtained in the channel with maximum fluorescence signal:

$$M_{km} = \frac{R_{km}}{R_{k\,max}}, R_{k\,max} = \max\{R_{k1}, R_{k2}, R_{k3}, R_{k4}\} \qquad (15)$$

$$M_{km}^{LIN} = \frac{R_{km}^{LIN}}{R_{k\,max}^{LIN}}, R_{km\,max}^{LIN} = \max\left\{R_{k1}^{LIN}, R_{k2}^{LIN}, R_{k3}^{LIN}, R_{k4}^{LIN}\right\} \qquad (16)$$

Values of M_{km} and M_{km}^{LIN}, m = 1, 2, 3, 4 represent a column of the cross-talk matrix estimated for one dye at the light intensity level k. Figure 7 shows values of M_{km} and M_{km}^{LIN} *versus* count rate $R_{k\,max}$ and $R_{k\,max}^{LIN}$. It is important to emphasize, that the distortion of the transfer matrix will be larger for spectral ranges which correspond to the tail of the fluorescence emission spectrum (see Fig. 7). This is due to the dependence of the SPD nonlinearity on the count rate. Indeed, for smaller count rates, nonlinearity will be insignificant while it will be substantial for higher count rates. Obviously, this will affect the normalized fluorescence response M_{km} (the higher the difference between R_{km} and $R_{k\,max}$, the bigger the distortion of the cross-talk matrix will be). Analysis of Fig. 7 shows that while nonlinearity above 15% substantially affects the cross-talk matrix obtained using nonlinearized data, linearization allows recovering the matrix values accurately for nonlinearity up to 60–80%.

In conclusion we have described nonlinear behavior and performance limitations of fluorescence detection systems based on single-photon counting. Experimental methods, physical models, and computational methods

for nonlinearity characterization, modeling, and compensation have been proposed enabling accurate description of SPD nonlinear behavior. We have demonstrated a nonlinear distortion of the cross-talk matrix caused by the SPD nonlinearity and implemented a data processing routine which enabled an accurate restoration of the cross-talk matrix for nonlinearity up to 50–60%.

4 References

[1] Lu, X., Yeung, E. S., *Appl. Spectrosc.* 1995, *49*, 605–609.

[2] Wang, Y., Wallin, J. M., Ju, J., Sensabaugh, G. F., Mathies, R. A., *Electrophoresis* 1996, *17*, 1485–1490.

[3] Kheterpal, I., Scherer, J. R., Clark, S. M., Radhakrishnan, A., Ju, J., Ginther, C. L., Sensabaugh, G. F., Mathies, R. A., *Electrophoresis* 1996, *17*, 1852–1859.

[4] Wang, Y., Hung, S. H., Linn, J. F., Steiner, G., Glazer, A. N., Sidransky, D., Mathies, R. A., *Electrophoresis* 1997, *18*, 1742–1749.

[5] Scherer, J. R., Kheterpal, I., Radhakrishnan, A., Ja, W. W., Mathies, R. A., *Electrophoresis* 1999, *20*, 1508–1517.

[6] Pang, H. M., Pavski, V., Yeung, E. S., *J. Biochem. Biophys. Methods* 1999, *41*, 121–132.

[7] Lu, S. X., Yeung, E. S., *J. Chromatogr. A* 1999, *853*, 359–369.

[8] Zhang, J. Z., Voss, K. O., Shaw, D. F., Roos, K. P., Lewis, D. F., Yan, J., Jiang, R., Ren, H., Hou, J. Y., Fang, Y., Puyang, X., Ahmadzadeh, H., Dovichi, N. J., *Nucleic Acids Res.* 1999, *27*, E36–E43.

[9] Crabtree, H. J., Bay, S. J., Lewis, D. F., Coulson, L. D., Fitzpatrick, G., Harrison, D. J., Delinger, S. L., Zhang, J. Z., Dovichi, N. J., *Electrophoresis* 2000, *21*, 1329–1335.

[10] Behr, S., Matzig, M., Levin, A., Eickhoff, H., Heller, C., *Electrophoresis* 1999, *20*, 1492–1507.

[11] Schmaltzing, D., Adourian, A., Koutny, L., Ziaugra, L., Matsudaira, P., Ehrlich, D., *Anal. Chem.* 1998, *70*, 2303–2310.

[12] Salas-Solano, O., Schmaltzing, D., Koutny, L., Buonocore, S., Adourian, A., Matsudaira, P., Ehrlich, D., *Anal. Chem.* 2000, *72*, 3129–3137.

[13] Koutny, L., Schmaltzing, D., Salas-Solano, O., El-Difrawy, S., Adourian, A., Buonocore, S., McEwan, P., Matsudaira, P., Ehrlich, D., *Anal. Chem.* 2000, *72*, 3388–3391.

[14] Wolley, A. T., Mathies, R. A., *Anal. Chem.* 1995, *67*, 3676–3680.

[15] Liu, S., Shi, Y., Ja, W. W., Mathies, R. A., *Anal. Chem.* 1999, *71*, 566–573.

[16] Medintz, I. L., Paegel, B. M., Blazej, R. G., Emrich, C. A., Berti, L., Scherer, J. R., Mathies, R. A., *Electrophoresis* 2001, *22*, 3845–3856.

[17] Papageorgas, G., Winter, H., Albrecht, H., *et al.*, *IEEE Trans. Instrum. Measurem.* 1999, *48*, 1166–1177.

[18] Tiberg, Y. E., Paulauskas, V. N., *Instrum. Exp. Tech.* 1981, *23*, 1252–1255.

[19] Evtyushenkov, A. M., Kiyachenko, Y. F., Olefirenko, G. I., Yudin, I. K., *Instrum. Exp. Tech.* 1982, *24*, 1265–1267.

[20] Shelevoi, K. D., *Instrum. Exp. Tech.* 1985, *28*, 614–616.

[21] Dovichi, N. J., Martin, J. C., Jett, J. H., Trkula, M., Keller, R. A., *Anal. Chem.* 1984, *56*, 348–354.

[22] Chen, D. Y., Dovichi, N. J., *Anal. Chem.* 1996, *68*, 690–696.

[23] Soper, S. A., Davis, L. M., Shera, E. B., *J. Opt. Soc. Am. B* 1992, *9*, 1761–1769.

[24] Soper, S. A., Mattingly, Q. L., Vegunta, P., *Anal. Chem.* 1993, *6*, 740–747.

[25] Alaverdian, L., Alaverdian, S., Bilenko, O., Bogdanov, I., Domrachev, S., Filippova, E., Gavrilov, D., Gorbovitski, B., Gouzman, M., Gudkov, I., Lifshitz, N., Luryi, S., Ruskovoloshin, V., Stepukhovich, A., Tcherevishnik, M., Tyshko, G., Gorfinkel, V., *Abstract Book „Advances in Genome Biology and Technology"*, Marco Island, FL, USA February 3–6 2001, p. 47.

[26] Alaverdian, L., Alaverdian, S., Bilenko, O., Bogdanov, I., Filippova, E., Gavrilov, D., Gorbovitski, B., Gouzman, M., Gudkov, G., Domratchev, S., Kosobokova, S., Lifshitz, N., Luryi, S., Ruskovoloshin, V., Stepoukhovitch, A., Tcherevishnick, M., Tyshko, G., Gorfinkel, V., *Electrophoresis* 2002, *23*, 2804–2817.

[27] Bedard, G., *Proc. Phys. Soc.*, 1967, *90*, 131–141.

[28] Gavrilov, D., *Dissertation Thesis*, State University of New York, Stony Brook 2002.

[29] Cummins, H. Z., Pike, E. R., *Photon Correlation and Light Beating Spectroscopy*, Plenum Press, New York 1973.

[30] Yin, Z., Severin, J., Giddings, M., Huang, W., Westphall, M. S., Smith, L. M., *Electrophoresis* 1996, *17*, 1143–1150.

Addendum 1

Derivation of characteristics for Model II: PDF of time τ between consecutive arriving photons $f_T(\tau)$ have the exponential distribution:

$$f_T(\tau) = R \exp\{-R\tau\} \tag{A1.1}$$

where R is rate of photon arrival. For SPD with temporal resolution τ_{res}, probability that each individual photon is registered P_{reg} at photon arrival rate R:

$$P_{reg} = P_T(\tau > \tau_{res}) = R\int_{\tau_{res}}^{\infty} \exp\{-R\tau\}d\tau = \exp\{-R\tau_{res}\} \tag{A1.2}$$

Then the rate of registered photons is found as

$$R_{reg} = P_{reg} R = R \exp\{-R\tau_{res}\} \tag{A1.3}$$

Addendum 2

Derivation of characteristics for Model III: In this model, the system is defined as having two states: 'high' state, characterized by resolution τ_H, and 'low' state with 'dead' time τ_L. Effective 'dead' time in 'high' state can be found as

$$\tau_H^* = P_{loss}\bar{\tau} + P_{loss}^2\bar{\tau} + P_{loss}^3\bar{\tau} + \ldots = \bar{\tau}\sum_{n=1}^{\infty} P_{loss}^n \tag{A2.1}$$

where $\bar{\tau} = R^{-1}$ is mean value of intervals between arriving photons, and P_{loss} is the probability of count loss in a system with temporal resolution τ_H at the photon arrival rate R, that can be found from Eq. (A1.2) as

$$P_{loss} = 1 - P_{reg} = 1 - \exp\{-R\tau_H\} \tag{A2.2}$$

Substituting Eq. (A2.2) into Eq. (A2.1) gives closed form expression for τ_H^*:

$$\bar{\tau}_H^* = \bar{\tau}\sum_{n=1}^{\infty} [1 - \exp\{-R\tau_H\}]^n = \frac{\exp\{R\tau_H\} - 1}{R} \tag{A2.3}$$

Effective 'dead' time of the system τ_D^* combines effective 'dead' time of the system in 'high' state τ_H^* and 'dead' time of the system in 'low' state τ_L:

$$\tau_D^* = \tau_H^* + \tau_L \tag{A2.4}$$

Then, substituting τ_D by τ_D^* in Eq. (2) we obtain expression for R_{reg}:

$$R_{reg} = \frac{R}{1 + \tau_D^* R} = \frac{R}{R\tau_L + \{\exp\{R\tau_H\}} \tag{A2.5}$$